Dalton Transactions

ROYAL SOCIETY OF CHEMISTRY

PAPER

View Article Online
View Journal | View Issue

Cite this: *Dalton Trans.*, 2025, **54**, 8174

Synthesis of highly dispersible TiO_2 nanoparticles and their application in quantum dot light emitting diodes†

Botao Hu, Mengxin Liu, Xinan Shi* and Daocheng Pan *

Received 19th February 2025,
Accepted 14th April 2025

DOI: 10.1039/d5dt00410a

rsc.li/dalton

Metal oxide nanoparticles are commonly used as electron transport layers (ETLs) in quantum dot light emitting diodes (QLEDs) because of their wide band gap, high electron mobility, and appropriate conduction and valence band positions. Currently, nanoparticulate ZnO is the most successful electron transportation material in high-performance QLEDs. However, the positive aging effect is widely observed for ZnO-based QLEDs, as the instability of amphiprotic ZnO nanoparticles under acidic, basic, and moist conditions limits their applications. In this study, highly dispersible and alcohol-soluble TiO_2 nanoparticles are synthesized by using a non-hydrolytic sol–gel method, followed by a dimethyl sulfoxide post-treatment. The use of colloidal TiO_2 nanoparticles as an ETL yields optimal QLEDs, with a maximum external quantum efficiency of 12.03%, a highest luminance value of 103 420 cd m^{-2}, and a current efficiency of 18.06 cd A^{-1}. These results reveal that TiO_2 nanoparticles hold great potential as ETLs in future QLEDs.

1. Introduction

Colloidal quantum dots (QDs) are widely used in optoelectronic devices due to their desirable features, including narrow emission bandwidth, tunable emission color, high quantum yield, excellent photostability, and solution processability.[1–9] Quantum dot light-emitting diodes (QLEDs) are considered to be a highly promising technology in next-generation lighting and displays.[10–12] The performance of QLEDs has been significantly improved since 1994.[13] Conventional QLED devices are composed of a sandwich structure: cathode, electron transport layer (ETL), QD emitting layer, hole transport layer (HTL), and anode. The ETL is one of the most crucial components of the QLED device. The electron mobility, conduction and valence band positions, and band gap of the ETL significantly influence the performance and stability of the device.[14–19] Wide band-gap metal oxides, such as ZnO, TiO_2, and SnO_2 nanoparticles, have been widely used as the ETLs in QLED devices. In 2011,[20] inorganic ZnO nanoparticles were first used as ETLs in QLEDs due to their high electron mobility, high transmittance and tunable energy levels.[21,22] Currently, high-performance QLEDs with an EQE exceeding 20% are being successfully fabricated based on ZnO-based ETLs. However, the positive aging effect is widely observed for ZnO-based QLEDs, as the instability of amphiprotic ZnO nanoparticles under acidic, basic, and moist conditions limits their applications.[23–25] Additionally, the high electron mobility of ZnO nanoparticles will result in the injection of excess electrons and a charge transportation imbalance, thereby reducing the performance and stability of QLEDs.[25] Recently, thermally stable and moisture-insensitive TiO_2 nanoparticles have been considered as one of the most promising alternatives to ZnO nanoparticles.[26–29] Furthermore, the wide band gap of TiO_2 nanoparticles and the energy level of the conduction band bottom facilitate the injection of electrons, making TiO_2 nanoparticles promising candidates for ETL materials.[30–33]

TiO_2 is an important indirect and wide band gap semiconductor that has been widely applied in various optoelectronic devices, including QLEDs,[30–33] thin film solar cells,[34,35] and GaN-based LEDs.[36–38] In 2021, Wei *et al.* synthesized oleic acid-capped TiO_2 nanocrystals by a two-phase approach.[30] Oil-soluble TiO_2 nanocrystals were turned into alcohol-soluble ones by post-treatment with thionyl chloride ($SOCl_2$), and were used as the ETL to fabricate QLEDs having long-term air-stability. Kim *et al.* used Li-doped TiO_2 nano-

State Key Laboratory of Featured Metal Materials and Life-cycle Safety for Composite Structures, Guangxi Key Laboratory of Processing for Non-ferrous Metals and Featured Materials, MOE Key Laboratory of New Processing Technology for Nonferrous Metals and Materials, School of Resources, Environment and Materials, Guangxi University, Nanning 530004, China. E-mail: xashi@gxu.edu.cn, dcpan@gxu.edu.cn

†Electronic supplementary information (ESI) available: XRD patterns of TiO_2 nanoparticles with different reaction times. Photographs of DMSO-capped TiO_2 nanoparticle solutions with different concentrations. FT-IR spectra of TiO_2 nanoparticles with and without DMSO post-treatment. SEM and AFM images of DMSO-capped TiO_2 nanoparticle thin films. See DOI: https://doi.org/10.1039/d5dt00410a

particles as the ETL to prepare highly efficient and green QLEDs with a maximum brightness of 169 790 cd m^{-2} and an EQE of 10.27%.[31]

However, the performance of QLEDs based on TiO_2 nanoparticles is still significantly poorer than that of state-of-the-art ZnO nanoparticle-based QLEDs.[4] A large number of –OH groups and high concentration of oxygen vacancies on the surface of TiO_2 nanocrystals result in severe fluorescence quenching of the quantum dots and deterioration of device performance.[39,40] Most traditionally synthesized TiO_2 nanoparticles are produced using the hydrolysis sol–gel process or the hydrothermal method.[41–43] These methods usually require high temperatures to induce crystallization. In this work, we employed a typical non-hydrolytic sol–gel method to prepare TiO_2 nanoparticles.[44] By controlling the reaction conditions, TiO_2 nanoparticles with controllable particle sizes can be synthesized. Note that these as-prepared TiO_2 nanoparticles cannot be dispersed in ethanol, which means uniform and flat TiO_2-nanoparticle thin films cannot be fabricated. Therefore, dimethyl sulfoxide (DMSO) was used to improve the solubility of TiO_2 nanoparticles in ethanol by a post-treatment process. As a result, DMSO-capped TiO_2 nanoparticles not only reduce hydroxyl group content on the surface of TiO_2 nanoparticles, but also inhibit fluorescence quenching of quantum dots, thereby enhancing device efficiency and brightness. The use of DMSO-capped TiO_2 nanoparticles as the electron transport layer yields a maximum brightness of 106 789 cd m^{-2}, a current efficiency of 18.01 cd A^{-1}, and an EQE of 12.08% for red-inverted QLED devices. These results suggest that TiO_2 nanoparticles have a significant potential to replace ZnO nanoparticles as the electron transport layer in QLEDs.

2. Experimental section

2.1 Chemicals

Molybdenum trioxide (MoO_3, 99.95%) and anhydrous ethanol (GR, 99.8%) were purchased from Aladdin Inc. 4,4′-*N*,*N*′-Dicarbazole-biphenyl (CBP, 99.5%) was bought from PolyLumTec Inc. Titanium tetrachloride ($TiCl_4$, 99.9%) and dimethyl sulfoxide (DMSO, 99%) were purchased from Macklin Inc. Red-emitting CdSe/ZnSe/ZnS core/shell/shell quantum dots (10 mg mL^{-1} in hexane) was provided by Pujiafu OptoElectronics Co. Ltd. All chemicals and solvents were used directly without any further purification.

2.2 Synthesis of TiO_2 nanoparticles

TiO_2 nanoparticles were synthesized using a non-hydrolytic sol–gel method with some modifications.[44] First, 50 mL of benzyl alcohol was added to a conical flask. Then, 0.54 mL of titanium tetrachloride was slowly dropped into the benzyl alcohol solution under magnetic stirring. The mixture was stirred for 15 minutes, and then placed in an oil bath at 130 °C for different reaction times. After the reaction, the conical flask was cooled to room temperature. The white suspension was then transferred to a centrifuge tube. The mixture was centrifuged, and the supernatant was decanted to collect TiO_2 nanoparticles.

2.3 Preparation of DMSO-capped TiO_2 nanoparticle solutions

TiO_2 nanoparticles were dispersed in 30 mL of anhydrous ethanol, and 3 mL of DMSO was added. The solution was then treated in an ultrasonic bath until a clear and transparent solution was formed. Ethyl acetate was added to precipitate the DMSO-capped TiO_2 nanoparticles, followed by a centrifuge process. Finally, the DMSO-capped TiO_2 nanoparticles were dispersed in anhydrous ethanol to obtain a solution of approximately 25 mg mL^{-1} for QLED device fabrication.

2.4 Fabrication of QLEDs

An inverted QLED device consists of ITO (150 nm), TiO_2 (35 nm), QDs (20 nm), CBP (40 nm), MoO_3 (7 nm), and Al (100 nm), respectively. First, ITO was ultrasonicated in deionized water and ethanol, respectively. Afterwards, the ITO was dried under a nitrogen flow. Then, the TiO_2 nanoparticle solution was spin-coated onto the ITO substrate at 2500 rpm for 20 s, followed by an annealing process at 150 °C for 15 minutes. Next, the QD solution was spin-coated onto the TiO_2 nanoparticle thin film at 3000 rpm for 20 s and was annealed at 100 °C for 10 minutes. CBP (40 nm), MoO_3 (7 nm), and Al electrodes (100 nm) were subsequently thermally evaporated.

2.5 Characterization studies

X-ray diffraction (XRD) measurements were carried out using a Bruker D8 Advance diffractometer. The UV-vis absorption spectrum of TiO_2 nanoparticles was obtained on a Metash 5200 spectrophotometer. Transmission electron microscopy (TEM) images of TiO_2 nanoparticles were acquired using an FEI Tecnai G2 F20 instrument. Scanning electron microscopy (SEM) images were acquired using a high-resolution field emission scanning electron microscope (Hitachi, SU820). Fourier transform infrared (FT-IR) spectra were recorded using a Nicolet 50 model. The Fermi level and valence band maximum (VBM) of the TiO_2 nanoparticle thin film were measured using an ESCALAB 250XI+ UPS with a He I (21.21 eV) photon source. The current–voltage–luminance curves and current efficiency–voltage–external quantum efficiency curves of the QLED devices were simultaneously recorded using a commercial QLED measurement system (XPQY-EQE-Adv, Guangzhou Xi Pu Optoelectronics Technology Co., Ltd). It should be noted that the QLEDs were manufactured and characterized in air without encapsulation.

3. Results and discussion

TiO_2 nanoparticles, as an important metal oxide material, have been extensively studied since their discovery. There are various methods for preparing TiO_2 nanocrystals. In this study, we employed a previously reported non-hydrolytic sol–gel method with some improvements.[44] The TiO_2 nanocrystals

synthesized using this method offer several significant advantages, including their large-scale synthesis, air stability, extremely small size, and narrower size distribution. We experimentally demonstrated that TiO_2 nanoparticles synthesized by the non-hydrolytic sol–gel method can be highly dispersed in ethanol by a DSMO post-treatment process and the hydroxyl group content on the TiO_2 nanoparticle surface is reduced, thereby inhibiting quantum dot PL quenching. These improved properties enable high-performance QLEDs based on a TiO_2 nanoparticle ETL.

All TiO_2 nanoparticles in this study were synthesized at low temperature without high-temperature post-annealing treatment. Fig. 1a and b show low-resolution TEM (LR-TEM) and high-resolution TEM (HR-TEM) images of DMSO-capped TiO_2 nanoparticles synthesized at 130 °C. A low-magnification overview image reveals that the product consists of discrete TiO_2 nanoparticles, with no larger agglomerates formed (see Fig. 1a). The high-resolution TEM image of the TiO_2 nanoparticle displays clear lattice streaks (see Fig. 1b), indicating that TiO_2 nanoparticles are highly crystalline. Based on the TEM images, the particle boundaries are clearly visible, and the particles exhibit a fairly uniform size and shape. The corresponding histogram of particle size distribution was generated (see Fig. 1c). The average particle size of TiO_2 nanocrystals was found to be 5.1 nm. This demonstrates that our final TiO_2 nanoparticles have extremely small size, narrow size distribution, and uniform shape. The X-ray diffraction (XRD) pattern of TiO_2 nanoparticles synthesized at 130 °C is shown in Fig. 1d. Specifically, the characteristic XRD peaks at 25.3, 37.8, 48.1, 55.6, and 62.7° correspond to diffraction from the (101), (004), (200), (211) and (204) crystal planes, respectively. These XRD peaks match those of the standard anatase structure of TiO_2 (JCPDS no. 21-1272). All peaks are attributed to the anatase phase, with no other peaks of impurities. Moreover, the broad diffraction peaks verify the small particle size of the as-synthesized TiO_2 nanoparticles. The particle size of the TiO_2 nanoparticles was determined by using the Scherrer diffraction formula, and the crystal size was calculated to be 4.9 nm, slightly smaller than the 5.1 nm size measured from the TEM image. These results suggest that the prepared TiO_2 nanoparticles have significant potential for use as the electron transport layer in QLEDs. Furthermore, we also

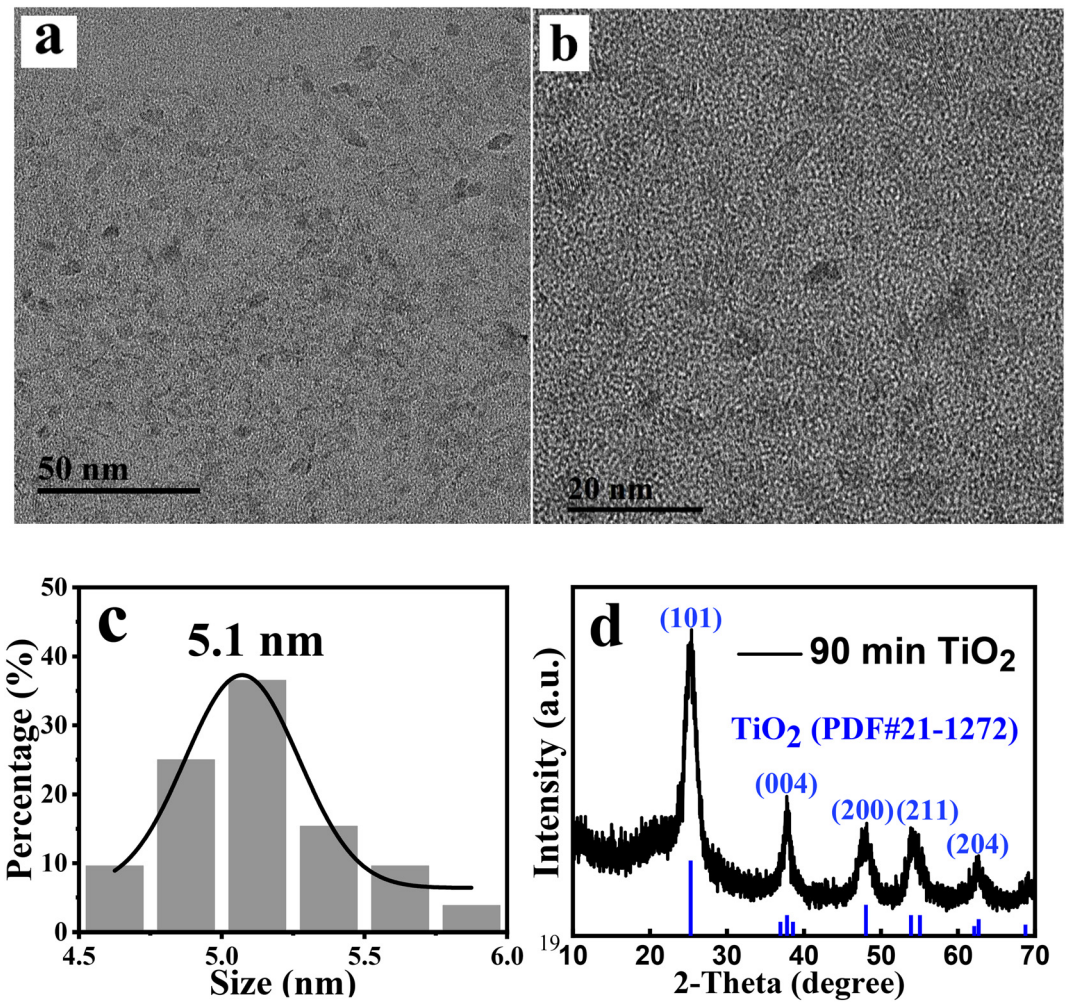

Fig. 1 (a) LR-TEM and (b) HR-TEM images; (c) the size distribution, and (d) XRD patterns of TiO_2 nanoparticles synthesized at 130 °C for 90 min.

investigated the effect of different reaction times on the particle size of the TiO_2 nanocrystals and found that TiO_2 nanocrystals can be produced in about 25 minutes at 130 °C in an oil bath. By controlling the reaction time, the particle size of TiO_2 nanoparticles can be adjusted from 4.4 to 5.9 nm, as shown in Fig. S1.† Raman spectra of as-prepared and DMSO-capped TiO_2 nanoparticles were recorded and are shown in Fig. S2.† The Raman characteristic peaks at 150, 397, 517, and 640 cm^{-1} are observed, corresponding to the anatase phase of TiO_2. This result is consistent with that of the XRD analysis, confirming that the TiO_2 nanoparticles have pure anatase structure.

Note that the as-prepared TiO_2 nanoparticles cannot be dispersed in ethanol. Therefore, DMSO was used to improve the solubility of TiO_2 nanoparticles in ethanol by a post-treatment process. DMSO-capped TiO_2 nanoparticles can be highly dispersed in ethanol, and a transparent and clear TiO_2 nanoparticle solution is formed, as shown in Fig. S3.† DMSO on the surface of TiO_2 nanoparticles has been confirmed by the FT-IR spectrum of TiO_2 nanoparticles (see Fig. S4†). Fig. 2a displays the UV-vis absorption spectrum of the TiO_2 nanocrystal solution, which exhibits an absorption peak at 292 nm and an absorption band edge at 375 nm. The optical band gap of TiO_2 nanocrystals was determined to be 3.93 eV from the UV-vis absorption curve, as shown in Fig. 2b. This value is significantly larger than the band gap value of bulk anatase TiO_2, which is 3.2 eV. Fig. S5 and S6† present a SEM image and an AFM image of the TiO_2 nanoparticle thin film, respectively. The TiO_2 nanoparticle thin film exhibits an average roughness (R_a) of 3.4 nm, which enables the deposition of smooth and flat TiO_2 thin film by a spin-coating process.

The Fermi level and valence band maximum (VBM) position were measured using ultraviolet photoelectron spectroscopy (UPS), as shown in Fig. 3. The VBM was calculated using the formula VBM = 21.21 − (E_{cutoff} − E_{onset}), where E_{cutoff} is the cut-off binding energy, and E_{onset} is the onset binding energy. The VBM of TiO_2 nanocrystals is calculated to be 7.87 eV below the vacuum energy level. Using the band gap

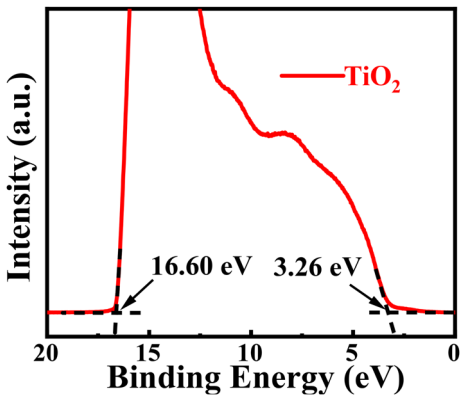

Fig. 3 UPS spectrum of the secondary-electron cutoff and valence-band edge regions of TiO_2 nanoparticles.

value E_g = 3.93 eV taken from Fig. 2b, the conduction band minimum (CBM) energy level of the DMSO-capped TiO_2 nanoparticles is estimated to be 3.94 eV below the vacuum energy level. The CBM energy level (−3.94 eV) of TiO_2 nanoparticles matches the ITO substrate, thereby facilitating smooth electron transport from ITO to the TiO_2 nanoparticle ETL. Furthermore, its deep VBM energy level (−7.87 eV) can effectively block holes at the interface between the EML and the ETL, confining the electron and hole to the QD emitting layer.[29]

The electron mobilities of TiO_2 and ZnO nanoparticles were determined using Child's law by fitting the space charge-limiting current (SCLC) region ($J \propto V^2$).[45] Fig. 4a and b show the current density–voltage (J–V) characteristic curves of TiO_2-based and ZnO-based nanoparticle films (ITO/TiO_2/Al and ITO/ZnO/Al). Using the equation from the literature,[45] $J = \frac{\left(\frac{9}{8}\right)\varepsilon_r\varepsilon_0\mu_e V^2}{d^3}$, and assuming $\varepsilon_r(TiO_2)$ = 85 and $\varepsilon_r(ZnO)$ = 4, the electron mobilities of TiO_2-based and ZnO-based nanoparticles were calculated as being $\mu = 3.77 \times 10^{-5}$ cm^2 V^{-1} s^{-1} and $\mu = 9.15 \times 10^{-3}$ cm^2 V^{-1} s^{-1}. We also tested the band gap,

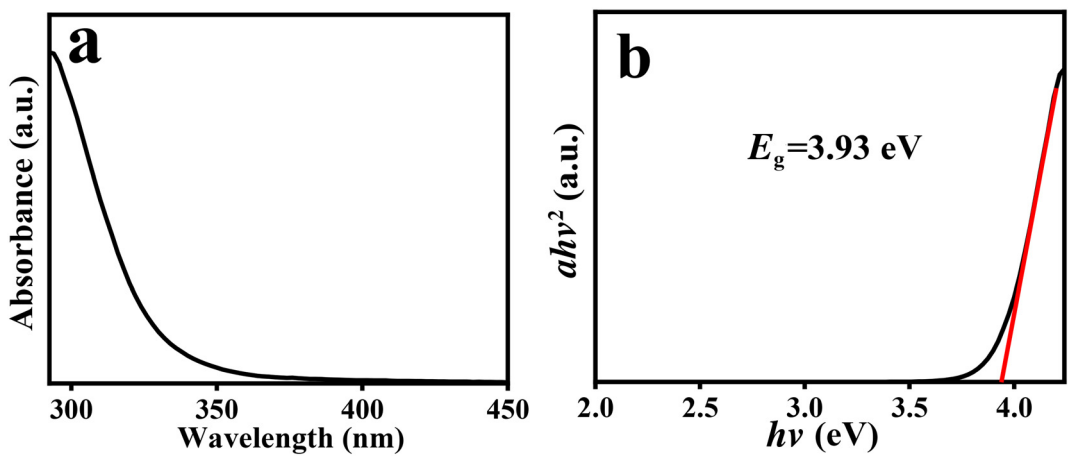

Fig. 2 (a) UV-vis absorption spectrum and (b) $(\alpha hv)^2$–hv plot (converted from the absorption spectrum) of DMSO-capped TiO_2 nanoparticles.

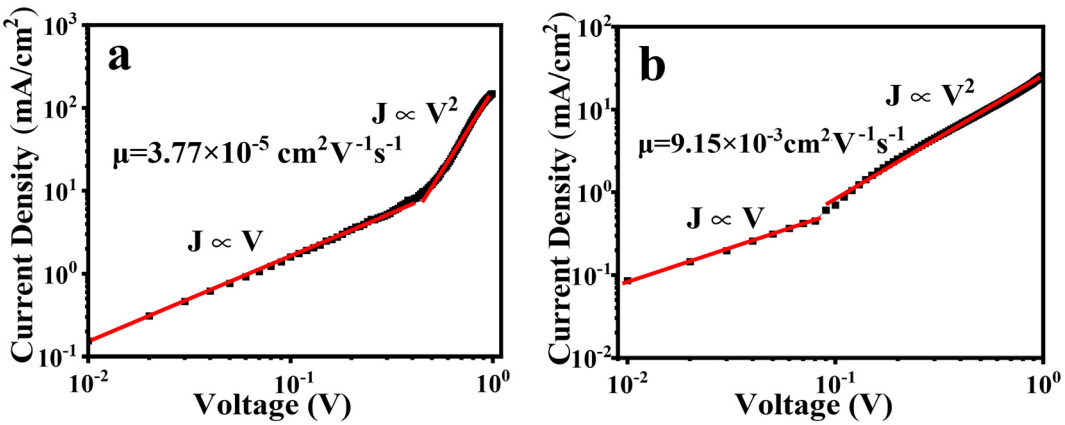

Fig. 4 Current density–voltage curves of (a) ITO/TiO_2/Al and (b) ITO/ZnO/Al devices.

Table 1 Comparison of the band gap, mobility and conductivity of ZnO and TiO_2 nanocrystal thin films, and CBP

	Band gap (eV)	Mobility ($cm^2\ V^{-1}\ s^{-1}$)	Conductivity ($S\ cm^{-1}$)
ZnO	3.65	9.15×10^{-3}	1.35×10^{-5}
TiO_2	3.93	3.77×10^{-5}	4.52×10^{-6}
CBP	3.10	5.78×10^{-5}	1.22×10^{-9}

conductivity, and hole mobility of CBP, as shown in Table 1. The mobility and conductivity of CBP are 5.78×10^{-5} $cm^2\ V^{-1}\ s^{-1}$ and 1.22×10^{-9} S cm^{-1}, respectively. Note that the electron mobility of ZnO nanoparticles is higher than the hole mobility of CBP by two orders of magnitude, which indicates a charge transportation imbalance in the ITO/ZnO/QD/CBP/MoO_3/Al device. It was found that the electron mobility of TiO_2 nanoparticles is of the same order of magnitude as the hole mobility of CBP. Therefore, TiO_2 nanoparticles are more suitable as an electronic transport layer than ZnO nanoparticles. This facilitates a better balance of charge carrier transport when TiO_2 nanoparticles are used in electron transport layers.

XPS was conducted to investigate the impact of the DMSO ligand on the electrical properties of TiO_2 nanocrystals. The as-prepared and unmodified TiO_2 nanocrystals, which cannot be dispersed in ethanol, form a turbid solution as shown in Fig. S7.† Compared with unmodified TiO_2 nanocrystals, DMSO-capped TiO_2 nanocrystals can be highly dispersed in ethanol. Each XPS O 1s spectrum shown in Fig. 5a or b reveals an asymmetric peak that can be fitted with two symmetric Gaussian peaks, and these two O 1s peaks are ascribed to the lattice oxygen (O–Ti) and surface hydroxyl (–OH) oxygen, respectively. It was found that DMSO post-treatment can lead to a notable reduction in surface hydroxyl (–OH) oxygen content from 37.36% to 30.08%, thereby inhibiting quantum dot PL quenching and improving the performance of QLEDs. According to the literature reports,[39,40] the quantum dot PL quenching mainly results from surface hydroxyl (–OH) oxygen.

The schematic structure of an inverted QLED device is presented in Fig. 6a. The QLED device consists of ITO/TiO_2 nanoparticles (35 nm), QDs (20 nm), CBP (40 nm), MoO_3 (7 nm), and Al (100 nm). Inverted QLED devices exhibit superior electroluminescent properties compared to conventionally structured QLED devices.[46,47] These properties include low turn-on voltage, high brightness, and high external quantum efficiency. As shown in the energy band diagram in Fig. 6b, there is a small injection barrier between the Fermi level of the ITO electrode and the CBM position of the TiO_2 nanoparticles, allowing efficient electron injection. The small potential barrier between the VBMs of CBP and MoO_3 allows for easy hole injection from the Al electrode into the quantum dot layer.

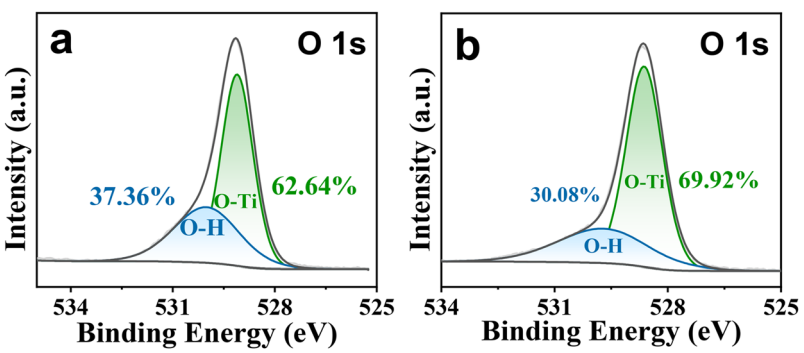

Fig. 5 XPS O 1s spectra of (a) unmodified TiO_2 nanocrystals and (b) DMSO-capped TiO_2 nanocrystals.

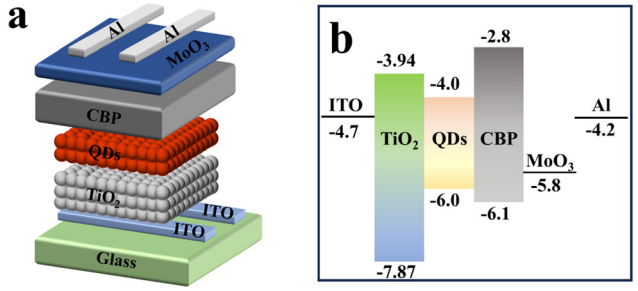

Fig. 6 The schematic structure of (a) the TiO_2 nanoparticle-based QLED device and (b) the corresponding energy band diagram of the inverted QLED.

Fig. 7a and b show the voltage-dependent current density, brightness, current efficiency, and EQE curves of a DMSO-capped TiO_2 nanocrystal-based QLED device. The experimental results reveal that when TiO_2 nanocrystals are used as the ETL, the device achieves a maximum brightness of 103 420 cd m^{-2}, a current efficiency of 18.06 cd A^{-1}, and an EQE of 12.03%. Notably, this is the highest efficiency achieved for the QLED device with a TiO_2 electron transport layer. In order to verify the reproducibility between batches, we fabricated 55 QLED devices in 13 batches. The EQE histogram in Fig. 7c shows an average EQE of 10.48%, with the highest EQE of 12.03%. It should be noted that our QLED devices were fabricated and tested directly in air (60% humidity, 25 °C) without any encapsulation. For comparison, ZnO nanoparticle-based QLEDs were also fabricated and characterized under the same conditions. No significant difference in current efficiency or EQE was observed between the two types of QLEDs. The current efficiency of a TiO_2-based QLED (18.01 cd A^{-1}) is slightly lower than that of a ZnO-based QLED (20.01 cd A^{-1}), while the maximum brightness of 103 420 cd m^{-2} for the TiO_2-based QLED is also only slightly lower than that of ZnO-based QLEDs (113 206 cd m^{-2}). Moreover, the EQEs for both QLEDs are quite similar. Transient electroluminescence spectra of TiO_2- and ZnO-based QLED devices were recorded and shown in Fig. 7d. It was found that the ZnO-based QLED demonstrates a faster rise in electroluminescence compared to the TiO_2-based device, indicating that electron transportation and injection in the TiO_2-based QLED device is weaker than that in the ZnO-based device, which is consistent with the results of the mobility experiments. Although the performance of our TiO_2-based QLED is inferior to that of state-of-the-art ZnO-based devices,[4] the EQE value of our TiO_2-based QLED is still the highest when compared with previously reported TiO_2-based QLEDs (see Table S1†). These results demonstrate the significant application potential of our TiO_2-based QLEDs.

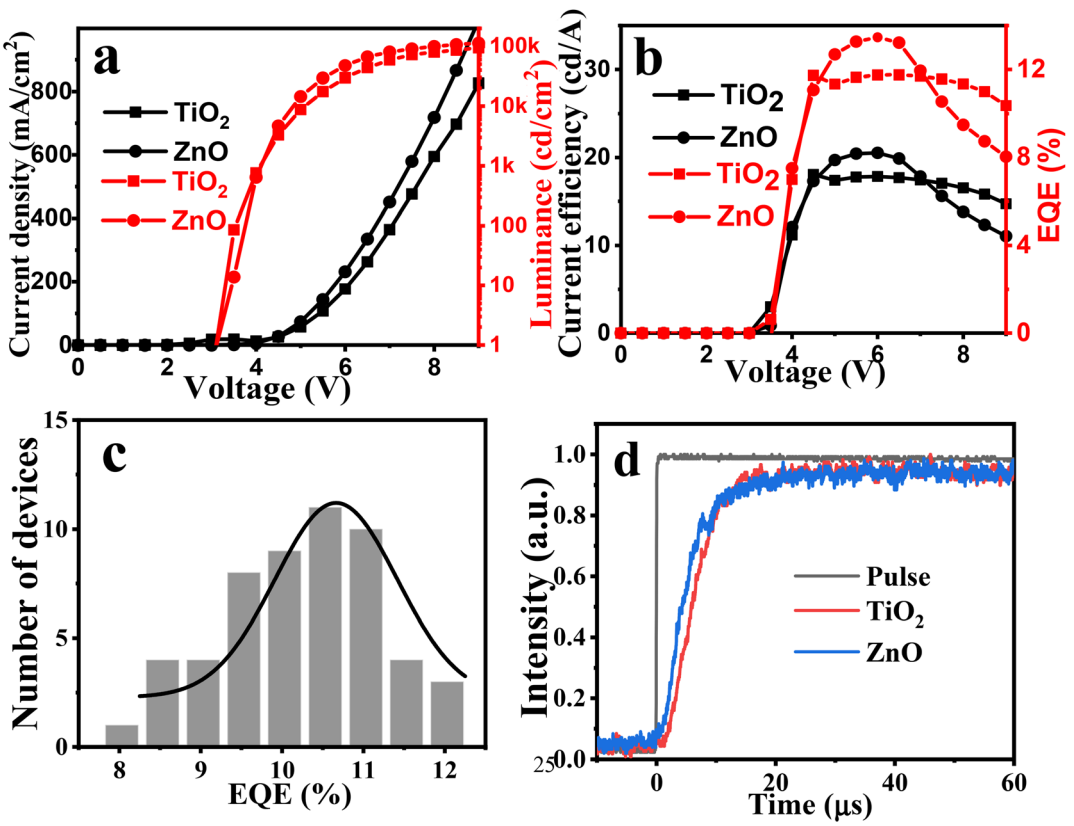

Fig. 7 (a) Current density–voltage–luminance (*J*–*V*–*L*) and (b) current efficiency–voltage–external quantum efficiency curves of the TiO_2-based QLEDs. (c) Histogram of the EQEs measured for 55 QLED devices. (d) The transient electroluminescence spectra of TiO_2- and ZnO-based QLED devices.

In order to further evaluate the potential application of the DMSO-capped TiO_2 nanocrystal ETL for cadmium-based QLEDs, we performed photoluminescence (PL) quenching experiments of CdSe/ZnSe/ZnS core/shell/shell quantum dot layers applied to spin-coated TiO_2 nanoparticle thin film and ZnO nanoparticle thin film. The results are as shown in Fig. 8. The pristine quantum dot film on the glass substrate exhibits the highest PL intensity, whereas a slight decrease in PL intensity was observed when the quantum dots were deposited on the ZnO nanoparticle thin film owing to a PL quenching phenomenon. This result is mainly attributed to the transfer of excitons from the QDs to ZnO nanoparticles. When the QDs were deposited on the film of DMSO-capped TiO_2 nanocrystals, the PL quenching observed was greater when compared with that of the ZnO nanoparticles, indicating that TiO_2 nanocrystals have a higher concentration of surface defects. The photoluminescence quenching efficiencies of ZnO and TiO_2 nanoparticles are 13.0% and 20.2%, respectively. This is the main reason why the performance of TiO_2 nanoparticle-based QLEDs is still significantly lower than that of state-of-the-art ZnO nanoparticle-based QLEDs.

Additionally, we investigated the stability of the TiO_2-based QLED device. For comparison, the ZnO-based QLED device was also fabricated and characterized under the same conditions (60% humidity, 25 °C). As shown in Fig. 9, the half-life of the unencapsulated ZnO-based QLED, with an initial brightness of 1006 cd m^{-2}, is 0.565 h. In contrast, the TiO_2-based QLED has a half-life of 2.56 h, which is five times longer than that of the ZnO-based QLED under the same conditions. This result indicates that the highly dispersible DMSO-capped TiO_2 nanoparticles can not only be used in high-performance QLED devices but they also meet the requirements of longer lifetime under air-aging conditions without encapsulation. Furthermore, the effect of encapsulation on the stability of the device was investigated. ZnO- and TiO_2-based QLEDs were simply encapsulated with ultraviolet-curing epoxy and a cover glass in air. Although the device stabilities of ZnO- and TiO_2-based QLEDs can be significantly improved by encapsulation (see Fig. S8†), the stabilities of TiO_2-based QLEDs are still significantly lower than those of state-of-the-art ZnO nanoparticle-based QLEDs.

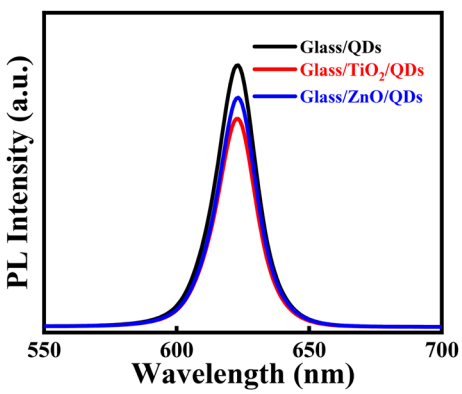

Fig. 8 Photoluminescence quenching experiments of CdSe QDs on glass, TiO_2 nanoparticle thin film, and ZnO nanoparticle thin film.

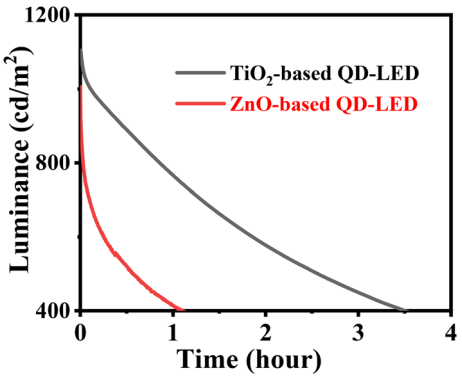

Fig. 9 The operational lifetime measurements of QLEDs based on TiO_2 and ZnO nanoparticles as the electron transportation layers. The devices were fabricated and monitored under ambient conditions of 60% relative humidity and 25 °C without encapsulation.

This is probably because our QLED devices are fabricated and encapsulated in air. Although the effect of water vapor on the stability of the device cannot be completely eliminated, our TiO_2-based QLED still exhibits greater stability than a ZnO-based device after encapsulation. These results show that DMSO-capped TiO_2 nanoparticles provide an effective means for achieving high-performance and air-stable QLEDs.

4. Conclusions

In summary, highly crystalline TiO_2 nanoparticles with a narrow size distribution were synthesized by a conventional non-hydrolytic sol–gel method. Post-treatment with DMSO resulted in the TiO_2 nanoparticles being highly dispersible in ethanol. QLEDs using TiO_2 nanoparticles as the electron transport layer achieved a maximum external quantum efficiency of 12.03%, a maximum luminance of 103 420 cd m^{-2}, and a current efficiency of 18.06 cd A^{-1}. Most importantly, these devices exhibited significantly improved lifetime and stability performances compared to ZnO-based QLED devices. TiO_2 nanoparticles, which are thermally stable, less sensitive to oxygen and moisture, and abundant in terms of their resources, are expected to replace ZnO nanoparticles as a more stable and efficient electron transport layer material in QLEDs.

Author contributions

B. T. Hu synthesized the nanocrystals and fabricated the QLEDs. X. A. Shi and M. Liu analyzed the experimental results. D. C. Pan designed the project. D. C. Pan and B.T. Hu wrote the manuscript.

Data availability

The data supporting this article have been included as part of the ESI.†

Conflicts of interest

There are no conflicts to declare.

Acknowledgements

This work was supported by the Special Fund for Science and Technology Development of Guangxi (grant no. AD25069078), the Guangxi Science and Technology Major Project (AA23073018), the Guangxi Natural Science Foundation (2023GXNSFDA026056), and the Guangxi Science and Technology Base and Talent Special Project (grant no. AD23026210).

References

1 Z. G. Xiao, R. A. Kerner, L. F. Zhao, N. L. Tran, K. M. Lee, T. W. Koh, G. D. Scholes and B. P. Rand, *Nat. Photonics*, 2017, **11**, 108–115.
2 M. K. Choi, J. Yang, D. C. Kim, Z. H. Dai, J. Kim, H. Seung, V. S. Kale, S. J. Sung, C. R. Park, N. S. Lu, T. Hyeon and D. H. Kim, *Adv. Mater.*, 2018, **30**, 1–7.
3 E. Jang and H. Jang, *Chem. Rev.*, 2023, **123**, 4663–4692.
4 Y. Gao, B. Li, X. Liu, H. Shen, Y. Song, J. Song, Z. Yan, X. Yan, Y. Chong, R. Yao, S. Wang, L. S. Li, F. Fan and Z. Du, *Nat. Nanotechnol.*, 2023, **18**, 1168–1174.
5 P. L. Gao, X. Y. Lan, J. H. Sun, J. H. Huang and Y. Zhang, *J. Mater. Sci.: Mater. Electron.*, 2020, **31**, 2551–2556.
6 T. Kim, K. H. Kim, S. Kim, S. M. Choi, H. Jang, H. K. Seo, H. Lee, D. Y. Chung and E. Jang, *Nature*, 2020, **586**, 385–389.
7 B. B. Yang, F. Zheng, S. L. Mei, Z. H. Chen, Y. Xie, H. Q. Dai, X. Wei, W. L. Zhang, F. X. Xie, J. Q. Ju, Y. Q. Chu, J. Zou and R. Q. Guo, *Appl. Surf. Sci.*, 2020, **512**, 1–9.
8 L. Q. Zhang, X. L. Yang, Q. Jiang, P. Y. Wang, Z. G. Yin, X. W. Zhang, H. R. Tan, Y. Yang, M. Y. Wei, B. R. Sutherland, E. H. Sargent and J. B. You, *Nat. Commun.*, 2017, **8**, 1–8.
9 X. L. Dai, Y. Z. Deng, X. G. Peng and Y. Z. Jin, *Adv. Mater.*, 2017, **29**, 1–22.
10 J. J. Song, O. Wang, H. B. Shen, Q. L. Lin, Z. H. Li, L. Wang, X. T. Zhang and L. S. Li, *Adv. Funct. Mater.*, 2019, **29**, 1808377.
11 Y. X. Yang, Y. Zheng, W. R. Cao, A. Titov, J. Hyvonen, J. R. Manders, J. G. Xue, P. H. Holloway and L. Qian, *Nat. Photonics*, 2015, **9**, 259–266.
12 C. Y. Xiang, L. J. Wu, Z. Z. Lu, M. L. Li, Y. W. Wen, Y. X. Yang, W. Y. Liu, T. Zhang, W. R. Cao, S. W. Tsang, B. Shan, X. L. Yan and L. Qian, *Nat. Commun.*, 2020, **11**, 1–9.
13 V. L. Colvin, M. C. Schlamp and A. P. Alivisatos, *Nature*, 1994, **370**, 354–357.
14 H. Y. Wang, H. L. Yu, W. D. Xu, Z. C. Yuan, Z. B. Yan, C. F. Wang, X. J. Liu, M. Fahlman, J. M. Liu, X. K. Liu and F. Gao, *J. Mater. Chem. C*, 2018, **6**, 6996–7002.
15 J. Chen, D. W. Zhao, C. Li, F. Xu, W. Lei, L. T. Sun, A. Nathan and X. W. Sun, *Sci. Rep.*, 2014, **4**, 1–6.
16 Y. Liu, S. Wei, G. Wang, J. Y. Tong, J. Li and D. C. Pan, *Langmuir*, 2020, **36**, 6605–6609.
17 K. P. Acharya, A. Titov, J. Hyvonen, C. G. Wang, J. Tokarz and P. H. Holloway, *Nanoscale*, 2017, **9**, 14451–14457.
18 A. Alexandrov, M. Zvaigzne, D. Lypenko, I. Nabiev and P. Samokhvalov, *Sci. Rep.*, 2020, **10**, 1–11.
19 S. Coe, W. K. Woo, M. Bawendi and V. Bulovic, *Nature*, 2002, **420**, 800–803.
20 L. Qian, Y. Zheng, J. G. Xue and P. H. Holloway, *Nat. Photonics*, 2011, **5**, 543–548.
21 J. Y. Pan, J. Chen, Q. Q. Huang, Q. Khan, X. Liu, Z. Tao, Z. C. Zhang, W. Lei and A. Nathan, *ACS Photonics*, 2016, **3**, 215–222.
22 D. Heo, J. H. Chang, D. Shin, J. Kwak, W. Bae and H. Lee, *Adv. Opt. Mater.*, 2023, **11**, 1–8.
23 Q. Su, Y. Z. Sun, H. Zhang and S. M. Chen, *Adv. Sci.*, 2018, **5**, 1–7.
24 W. J. Zhang, X. T. Chen, Y. H. Ma, Z. W. Xu, L. J. Wu, Y. X. Yang, S. W. Tsang and S. J. Chen, *Phys. Chem. Lett.*, 2020, **11**, 5863–5870.
25 W. K. Bae, Y. S. Park, J. Lim, D. Lee, L. A. Padilha, H. McDaniel, I. Robel, C. Lee, J. M. Pietryga and V. I. Klimov, *Nat. Commun.*, 2013, **4**, 1–8.
26 M. Quintana, T. Edvinsson, A. Hagfeldt and G. Boschloo, *J. Phys. Chem. C*, 2007, **111**, 1035–1041.
27 R. Jose, V. Thavasi and S. Ramakrishna, *J. Am. Ceram. Soc.*, 2009, **92**, 289–301.
28 K. Ellmer, *Nat. Photonics*, 2012, **6**, 808–816.
29 K. S. Cho, E. K. Lee, W. J. Joo, E. Jang, T. H. Kim, S. J. Lee, S. J. Kwon, J. Y. Han, B. K. Kim, B. L. Choi and J. M. Kim, *Nat. Photonics*, 2009, **3**, 341–345.
30 S. Wei, J. Miao, Q. Shi, S. Shao and L. Zhang, *J. Mater. Sci.: Mater. Electron.*, 2021, **32**, 9795–9803.
31 M. Kim, N. Lee, J. H. Yang, C. W. Han, H. M. Kim, W. Han, H. H. Park, H. Yang and J. Kim, *Nanoscale*, 2021, **13**, 2838–2842.
32 M. G. Kim, J. S. Shin, J. H. Ma, J. H. Jeong, D. H. Han, B. S. Kim, W. Jeon, Y. Park and S. J. Kang, *J. Mater. Chem. C*, 2022, **10**, 7294–7303.
33 C. Yoon and J. Kim, *J. Korean Inst. Met. Mater.*, 2023, **61**, 33–37.
34 H. Zhou, T. B. Song, C. H. Chung, B. Lei, B. Bob, R. Zhu, H. S. Duan, C. J. Hsu and Y. Yang, *Adv. Energy Mater.*, 2012, **2**, 1368–1374.
35 L. E. Greene, M. Law, B. D. Yuhas and P. D. Yang, *J. Phys. Chem. C*, 2007, **111**, 18451–18456.
36 P. F. Zhu, H. Y. Zhu, W. P. Qin, B. H. Dantas, W. Sun, C. K. Tan and N. Tansu, *J. Appl. Phys.*, 2016, **119**, 124305.
37 P. F. Zhu, G. Y. Liu, J. Zhang and N. Tansu, *J. Disp. Technol.*, 2013, **9**, 317–323.
38 X. H. Li, P. F. Zhu, G. Y. Liu, J. Zhang, N. Tansu, R. B. Song, Y.-K. Ee, P. Kumnorkaew, J. Gilchrist and N. Tansu, *J. Disp. Technol.*, 2013, **9**, 324–332.
39 S. Y. Yoon, Y. J. Lee, H. Yang, D. Y. Jo, H. M. Kim, Y. Kim, S. M. Park, S. Park and H. Yang, *ACS Energy Lett.*, 2022, **7**, 2247–2255.

40 M. Gao, Y. F. Tu, D. D. Tian, H. W. Yang, X. Y. Fang, F. J. Zhang, H. B. Shen and Z. L. Du, *ACS Photonics*, 2022, **9**, 1400–1408.
41 P. D. Cozzoli, A. Kornowski and H. Weller, *J. Am. Chem. Soc.*, 2003, **125**, 14539–14548.
42 A. R. Rao and V. Dutta, *Sol. Energy Mater. Sol. Cells*, 2007, **91**, 1075–1080.
43 Q. H. Zhang and L. Gao, *Langmuir*, 2003, **19**, 967–971.
44 M. Niederberger, M. H. Bartl and G. D. Stucky, *Chem. Mater.*, 2002, **14**, 4364–4370.
45 M. A. Lampert, *Phys. Rev.*, 1956, **103**, 1648–1656.
46 W. Xu, W. Y. Ji, P. T. Jing, X. Yuan, Y. A. Wang, W. D. Xiang and J. L. Zhao, *Opt. Lett.*, 2014, **39**, 426–429.
47 T. Lee, B. J. Kim, H. Lee, D. Hahm, W. K. Bae, J. Lim and J. Kwak, *Adv. Mater.*, 2022, **34**, 1–9.